nature physics

SUPPLEMENTARY INFORMATION

DOI: 10.1038/NPHYS3894

"Universality of pseudogap and emergent order in lightly doped Mott insulators"

I. Battisti[1]*, K.M. Bastiaans[1]*, V. Fedoseev[1], A. de la Torre[2,3], N. Iliopoulos[1], A. Tamai[2], E.C. Hunter[4], R.S. Perry[5], J. Zaanen[1], F. Baumberger[2,6], M.P. Allan[1¶]

[1] *Leiden Institute of Physics, Leiden University, Niels Bohrweg 2, 2333 CA Leiden, The Netherlands*
[2] *Department of Quantum Matter Physics, University of Geneva, 24 Quai Ernest-Ansermet, 1211 Geneva 4, Switzerland*
[3] *Department of Physics, California Institute of Technology, Pasadena, California 91125, USA*
[4] *School of Physics and Astronomy, The University of Edinburgh, James Clerk Maxwell Building, Mayfield Road, Edinburgh EH9 2TT, United Kingdom*
[5] *London Centre for Nanotechnology and UCL Centre for Materials Discovery, University College London, London WC1E 6BT, United Kingdom*
[6] *Swiss Light Source, Paul Scherrer Institute, CH-5232 Villigen PSI, Switzerland*
* *these authors contributed equally to this work;* ¶ *allan@physics.leidenuniv.nl*

1. Sample characterization

In this section we show resistivity data measured on the samples we studied. The sample growth technique is described in the *Methods* section of the main text.

Fig. S1 shows the resistivity curves for different dopant concentrations. Note that the rough La concentrations reported in the graph are determined by energy dispersive x-ray spectroscopy (EDX), and this method averages over variations of the doping concentration. We estimate these variations to occur on a length-scale of hundreds of micrometers, and the magnitude to be of the order of a few percentage points. These variations in doping concentrations have to be considered when interpreting resistivity (Figure S1) and magnetization data of the iridate samples.

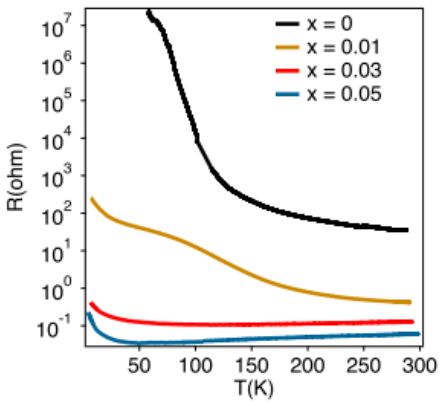

Fig. S1: The transition towards metallicity as a function of doping. Figure reproduced from Ref. [1].

2. Set-up effect in topographs

DOI: 10.1038/NPHYS3894

In all samples, we encounter a strong dependence of the topographs appearance on the set-up condition, due to the strong electronic inhomogeneity present in $(Sr_{1-x}La_x)_2IrO_4$. Because this inhomogeneity is present up to high bias voltages of order of electron-Volts, it is visible even if the topographs are set up around ~1V. While the topographs do not change strongly upon increasing the absolute value of the bias voltage, we report a strong asymmetry between positive and negative setup. With positive setup (Fig S2a), the dopants have local C_2 symmetry, they are more difficult to identify and they sit on a homogeneous background. With negative setup (Fig S2b), they have C_4 symmetry and we observe a substantial difference in the contrast between areas with/without dopants.

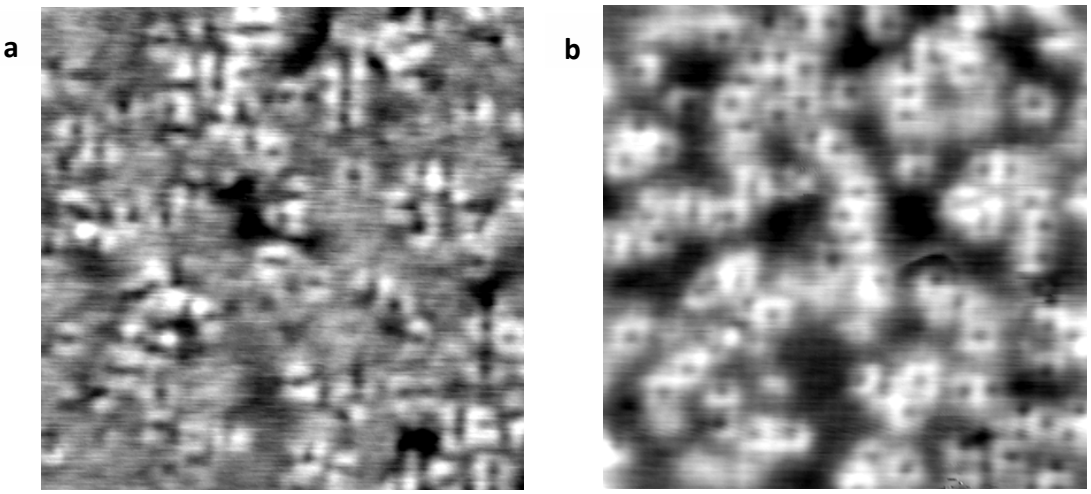

Fig. S2. Comparison between two topographs of doping level 5.4% measured on the same area with different setup conditions. (a) Field of view 11.4nm, (V_{bias}, $I_{setpoint}$)=(0.5V, 300pA). The dopants have C_2 symmetry and the background is homogeneous in contrast. (b)Field of view 11.4nm, (V_{bias}, $I_{setpoint}$)=(-0.7V, 800pA). The dopants have C4 symmetry and the background is inhomogeneous.

3. Identification of dopant atoms location

Identifying the location of the dopant atoms plays an important role in our analysis, and it is more challenging when the doping level is high. Here, we describe our method to count and localize the dopant atoms.

Given a topograph (Fig. S3a), we superimpose the atomic lattice obtained by Fourier filtering to mark the positions of Sr atoms (green in fig S3b). Using this grid, we identify the La dopant locations (red in figure S3b) which substitute Sr atoms.

In addition, we establish a procedure to find the dopant location in the spectroscopic map measurements. Due to the asymmetry of the setup effect, the topograph contains not only topographic information but also electronic inhomogeneity. While it is possible to identify the dopant positions in the unprocessed topographs (see Fig S3a, b, c), it becomes easier if we cancel part of the electronic inhomogeneity by summing the topograph (Fig S3c) with the integral of a certain number of layers in the opposite bias voltage region (Fig S3d). After filtering the resulting image we obtain what we call the processed image (Fig S3e). There, the impurities are most prominently visible.

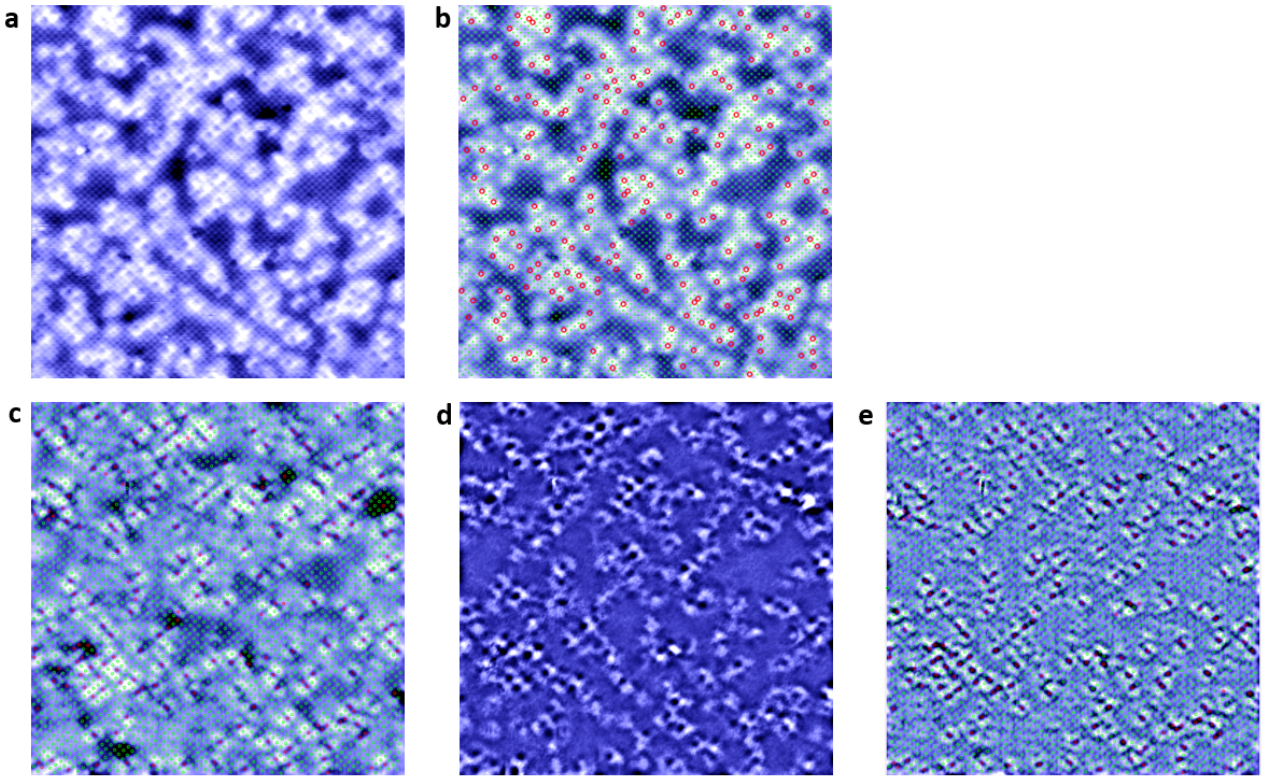

Fig. S3. **a**, Topograph in a field of view of 20 nm, with setup conditions (V_{bias}, $I_{setpoint}$)=(-0.75V, 400pA).**b**, Same topograph as in a, with Sr atoms in green and La atoms in red. **c**, Spectroscopic map, field of view 17 nm, (V_{bias}, $I_{setpoint}$)=(0.55V, 300pA). Topograph with with Sr atoms in green and La atoms in red. **d**, Integral of conductance layer from -900 meV to -450 meV. **e**, Resulting processed image with Sr atoms in green and La atoms in red.

4. Tip-induced band bending

When doing spectroscopy with STM on a metallic sample all the bias voltage drops in the vacuum gap between tip and sample. No voltage drops inside the sample due to the very short screening length of electric field, therefore the bias voltage applied to the sample equals the tip-sample vacuum gap voltage. The applied tip-sample voltage (bias) is equal, on the energy scale, to the distance from the Fermi level of a probed electronic state. On the other hand, in semiconductors [2-6] and Mott insulators [7], the screening length is not negligible. When performing spectroscopy on such samples, the voltage drop inside the sample, so called "tip induced band bending" (TIBB), must be taken into account to retrieve the relative energy of electronic states from the applied bias [2-5].

As our samples are poor conductors with non-metallic resistivity $\rho(T)$ curves (Fig. S1), we can assume that the TIBB should be taken into account. This is confirmed by the observation of semiconductor phenomenology in these samples with SI-STM (gapped density of states, TIBB "bubbles" [3]).

DOI: 10.1038/NPHYS3894

In this section we show that TIBB may result into the apparent band gap being much higher than the real energy gap for our samples.

To get a rough estimate of the voltage drop inside the sample V_{sample} one can consider a homogeneously charged sphere (charges are fixed on the surface) of radius R at a distance $L<<R$ from the sample, seen as a dielectric semi-space with relative permittivity ε without any free carriers (Fig. S4), and only assuming static fields. Straightforward electrostatic considerations give

$$V_{sample} = V_{bias} \frac{1}{1 + \varepsilon \frac{L}{R}} \qquad \text{(Equation 1)}$$

Where V_{bias} is defined as the voltage drop between the point on the sphere closest to the sample and a point infinitely far from it. As the sphere is located very close to the sample ($L<<R$), the tip charge redistribution must be taken into account. Thus a more realistic configuration is the one with a metallic sphere. Using the method of electrostatic images (a charge on the sphere induces an image charge in the sample and a charge in the sample induces an electrostatic image dipole on the sphere), this configuration can be solved numerically. To compare this solution to (Equation 1), it can be expressed as

$$V_{sample} = V_{bias} \frac{1}{1 + c\varepsilon \frac{L}{R}}$$

Where c is a slow varying function on ε and R/L; for example c=2.88 for ε=50, R/L=40. These values are chosen as we estimate L≈0.5nm, R≈15-50nm. To our best knowledge, static relative permittivity of undoped Sr_2IrO_4 is not available in literature, therefore we estimate it from [8,9] by taking the averaged values, obtaining ε_c ≈30 for $E||c$-axis and ε_{ab} ≈100 for $E||ab$ crystal plane.

Therefore, the charge redistribution on the sphere due to the sample proximity decreases the sample voltage drop V_{sample} via an increase of the electric field in the vacuum gap. This is contrary to a naïve expectation of V_{sample} increasing when charge on the sphere is attracted to the sample, causing L to become effectively smaller.

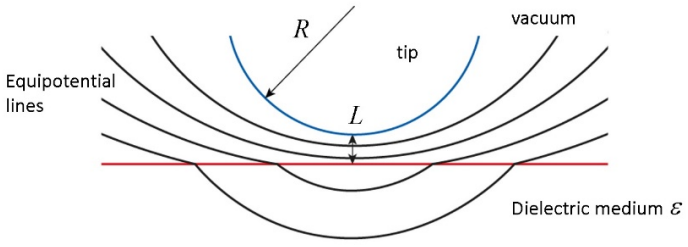

Fig. S4. Model to estimate voltage drop inside a non-metallic sample. Tip-sample voltage partly drops in the tip-sample vacuum gap and inside the sample. The tip is modelled by a sphere.

A model closer to an STM setup is a charged hyperbolic metallic surface with radius R at the apex and shank opening angle ~30° (2β) located at a distance L above the sample (Fig. S5).

This geometry can be solved by finding an appropriate set of a homogeneously charged semi-infinite straight line and a number of point charges between the sample and the line having equivalent boundary conditions to the initial configuration (Fig. S6) [10].

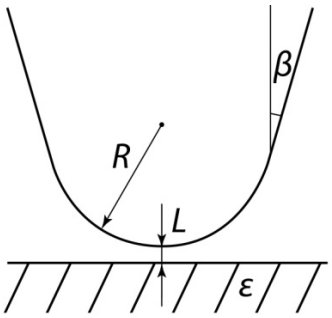

Fig. S5. A more appropriate model of the tip with hyperbolic shape.

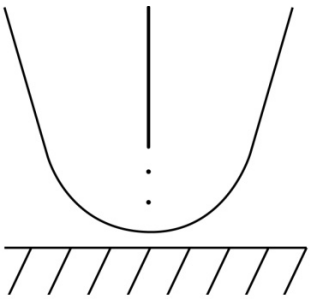

Fig. S6. A semi-infinite homogeneously charged line and a few appropriately chosen point charges above a dielectric semi-space have electrostatic fields distribution identical to the hyperbolic tip-sample geometry.

Numerical calculations show that such a geometry results in a ~20% increase of TIBB compared to the spherical metallic tip model. Finally, introduction of free carriers diminishes TIBB as free carriers screen electric field inside the sample.

The uncertainty of tip shape and poorly understood free carrier concentration in doped Mott insulators results in a big error bar for the sample voltage drop. Under assumption of a rather blunt tip and negligible free carrier concentration in lightly doped Sr_2IrO_4, TIBB can result in the apparent band gap being few times larger than the real energy gap.

5. Disordered stripy pattern

Below, we show a side-by-side comparison of disordered patterns in the conductance layers of iridates with underdoped cuprates. In BSCCO, the patterns are and, based on the limited

DOI: 10.1038/NPHYS3894

data that exist, get even more disordered when parts of the sample become more insulating. In our measurements, the pseudogap puddles are smaller than in the measurements on BSCCO and NaCCO, and we thus expect the disorder to be even stronger than in the previously published images.

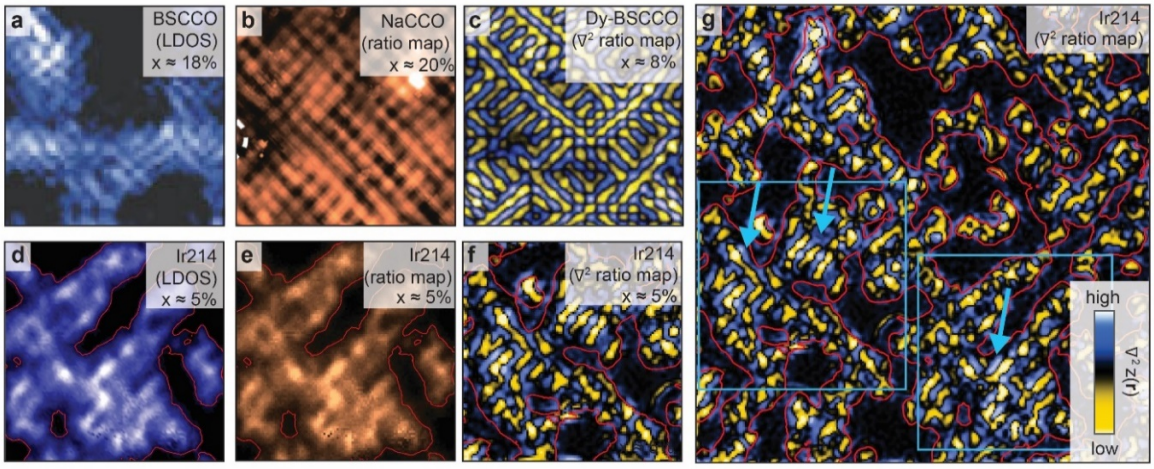

Fig S7 Disordered stripy pattern in the cuprates and the iridates. **a**,**b**,**c**, Disordered stripy pattern in BSCCO and NaCCO seen in the conductance, the ratio map, and the Laplacian of the ratio map, respectively (reproduced from [11, 12, 13]). **d**,**e**,**f**, The corresponding iridate samples exhibit even more disordered patterns likely because they correspond to lower doping. **g**, The larger the pseudogap puddle, the less disordered are the stripy pattern (blue arrows). The blue boxes indicate the regions in d,e,f.

6. Fitting procedures

In order to fit both spectra in the Mott region and in the pseudogap puddles, we develop a fitting procedure as follows (Fig. S8). We start with a smooth polynomial background density of states $DOS_{BG}(E) = aE^2 + c$, where E is the energy, and a and c are fitting parameters. Next, we multiply it with a phenomenological Mott gap Δ_{Mott} consisting of two slightly broadened gap edges, asymmetric around the chemical potential:

$$DOS_{Mott}(E) = \left| \frac{1}{1 + e^{(-E-E_0)/w}} - \frac{1}{1 + e^{(-E+E_0-\Delta_{Mott})/w}} \right|$$

The gap edges are broadened by w, E_0 is the energy where the upper Hubbard band roughly pins to the chemical potential and Δ_{Mott} is the size of the Mott gap. We keep the first two parameters fixed (w=0.026 eV, E_0=0.1 eV), while the size of the Mott gap Δ_{Mott} is used as a fitting parameter. We then allow for states inside the Mott gap that are gapped by introducing a phenomenological function based on photoemission results and commonly used in the cuprates [14,15]. This part allows for the extraction of the pseudogap value Δ_{PG}.

$$DOS_{PG}(E) = C_0 \left| \frac{E + i\alpha\sqrt{E}}{\sqrt{\left(E + i\alpha\sqrt{E}\right)^2 - \Delta_{PG}^2}} \right|$$

This function contains two fitting parameters: a scaling factor C_0 and the size of the pseudogap Δ_{PG}. We keep α, an effective scattering rate, fixed to $0.2eV^{0.5}$. The square root in the imaginary part of the self-energy is selected to ensure a rather constant broadening independent of the gap. The resulting model is an excellent fit to all the spectra measured on the highly doped samples, as it can be seen in Fig. S9 where we show 10 randomly chosen spectra with the corresponding fit.

Next to the pseudogap energy Δ_{PG} and the Mott gap energy Δ_{Mott}, our fitting routine also utilizes three other fitting parameters. As mentioned in the *Methods* section, these are the parameters *a* and *c* for the background density of states and the parameter C_0 which scales the V-shaped pseudogap function. In Fig. S10 we show the maps of these additional parameters corresponding to the Δ_{PG} map shown in the main text (Fig. 3e).

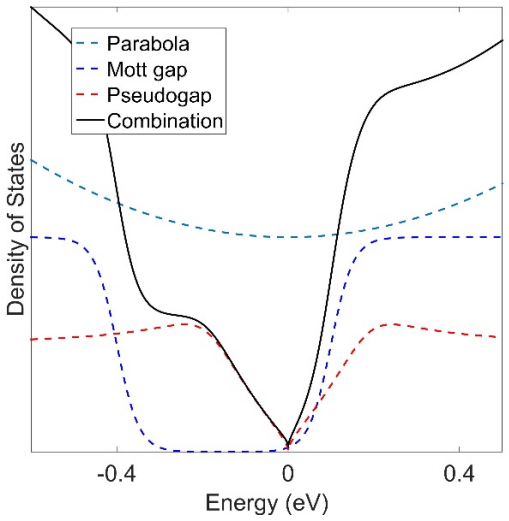

Fig. S8. Phenomenological fit function to simultaneously extract both the Mott and pseudogap size. It consists of a polynomial density of states (dashed light blue) multiplied with Mott gap (dashed blue) plus states inside the Mott gap with a v-shaped pseudogap (dashed red).

DOI: 10.1038/NPHYS3894

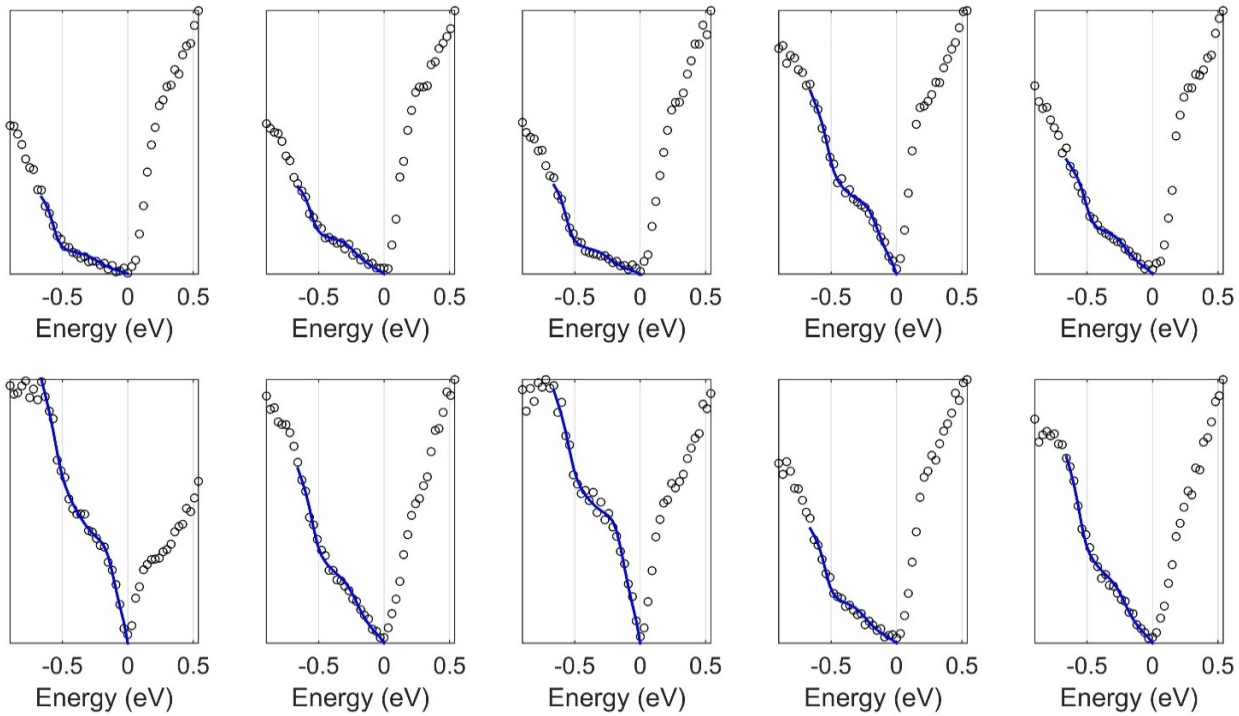

Fig. S9. Ten randomly selected curves from the dataset shown in Fig.3 in the text, fitted with the constructed fit function. The open dots represent the data points. The dark blue lines are fits to the data.

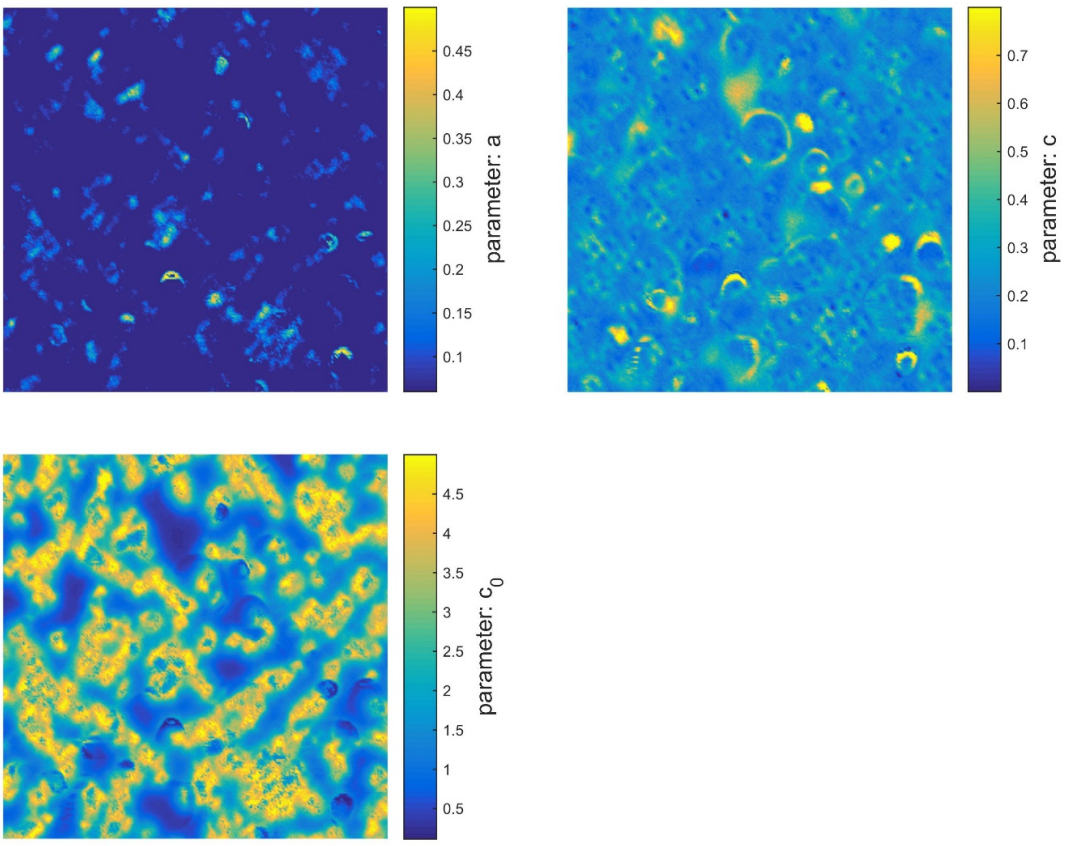

Fig. S10. Maps of additional fitting parameters, corresponding to the Δ_{PG} map shown in Figure 3 of the main text.

7. Mott gap map

Using the fitting procedure described in the previous paragraph, we are able to simultaneously extract the value of the Mott gap Δ_{Mott} and of the pseudogap Δ_{PG} for each spectrum in the spectroscopic maps. We can then plot Mott gap maps and pseudogap maps as in Fig. S11a,b. The extraction of the values of the two gaps allows us to calculate the correlation between the two gaps within the pseudogap puddles (Fig. S11c).

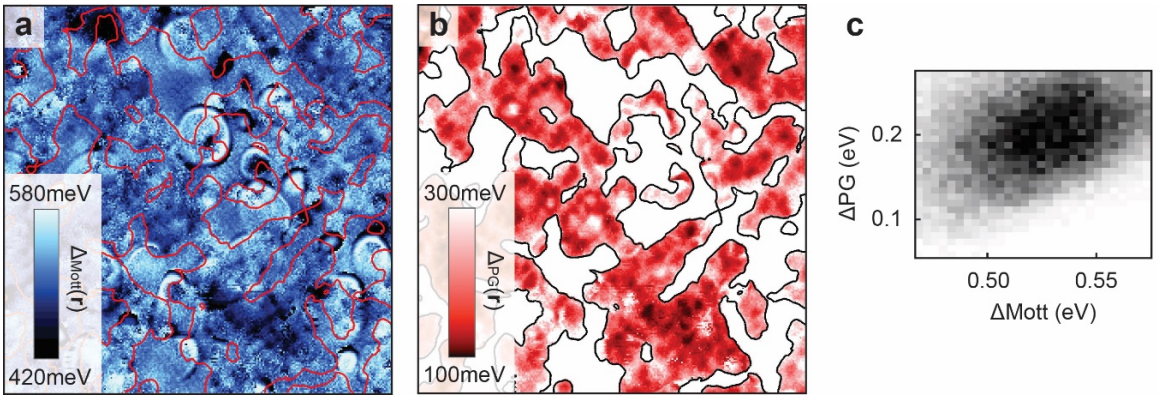

Fig. S11. Mott gap map and pseudogap map in a 17 nm field of view region (same measurement as Fig. 3 main text). **a**, Mott gap map. **b**, Pseudogap map. **c**, Correlation between Mott gap and pseudogap.

References

[1] de la Torre, A. *et al.*, *Phys. Rev. Lett.* **115,** 176402 (2015) Supplementary Information

[2] Feenstra, R. M., Stroscio, J. A. Tunneling spectroscopy of the GaAs(110) surface. J. Vac. Sci. Technol. B 5, 923 (1987).

[3] Wijnheijmer, A.P. *et al*. Enhanced Donor Binding Energy Close to a Semiconductor Surface. *Phys. Rev. Lett.* **102**, 166101 (2009).

[4] Loth, S. Atomic Scale Images of Acceptors in III-V Semiconductors. PhD Dissertation, Universität Göttingen (2008).

[5] Teichmann, K. Scanning tunneling spectroscopy of space charge regions in semiconductors : from single donor to heterostructure systems. PhD Dissertation, Universität Göttingen, (2012).

[6] Wijnheijmer, A.P. Manipulation and analysis of a single dopant atom in GaAs door. PhD Dissertation, Technische Universiteit Eindhoven (2011).

[7] Zhou, Y. & Ramanathan, S. Correlated electron materials and field effect transistors for logic: a review. Crit. Rev. Solid State Mater. Sci. **38**, 286–317 (2013).

[8] Chikara, S. *et al*. Giant magneto-electric effect in the J_{eff} = ½ Mott insulator Sr_2IrO_4. *Phys. Rev. B* **80**, 140407(2009).

[9] Varyukhin, S. V., ZAkharov, A. A. Anisotropic dielectric constant of La_2CuO_4. Physica C **185**, 975-976 (1991).

[10] Mesa, G., Dobado-Fuentes, E., Saenz, J. J. Image charge method for electrostatic calculations in field-emission diodes. J. Appl. Phys. **79**, 39, (1996).

DOI: 10.1038/NPHYS3894

[11] McElroy, K. et al. Relating atomic-scale electronic phenomena to wave-like quasiparticle states in superconducting Bi2Sr2CaCu2O8+delta. Nature **422**, 592–6 (2003).

[12] Hanaguri, T. et al. Quasiparticle interference and superconducting gap in Ca2−xNaxCuO2Cl2. Nat. Phys. **3**, 865–871 (2007).

[13] Kohsaka, Y. et al. An intrinsic bond-centered electronic glass with unidirectional domains in underdoped cuprates. Science **315**, 1380–5 (2007).

[14] Alldredge, J. W., et al. "Evolution of the electronic excitation spectrum with strongly diminishing hole density in superconducting $Bi_2Sr_2CaCu_2O_{8+\delta}$." *Nature Physics* **4**, 319-326 (2008)

[15] Kim, Y. K., Sung, N. H., Denlinger, J. D. & Kim, B. J. Observation of a *d*-wave gap in electron-doped Sr_2IrO_4. Nat. Phys. **12**, 1–6 (2015).